Solar Energy Materials & Solar Cells 210 (2020) 110519

Contents lists available at ScienceDirect

Solar Energy Materials and Solar Cells

journal homepage: http://www.elsevier.com/locate/solmat

Correlation between the open-circuit voltage and recombination loss at metal-silicon interfaces of crystalline silicon solar cells

Myeong Sang Jeong [a,b], Kwan Hong Min [a,b], Sungjin Choi [a,c], Min Gu Kang [a], Kyung Taek Jeong [a], Eun Tae Lee [d], Yoonmook Kang [c], Donghwan Kim [b,c], Hae-Seok Lee [c,***], Hee-eun Song [a,**], Sungeun Park [a,*]

[a] Photovoltaic Laboratory, Korea Institute of Energy Research, Daejeon, 34129, Republic of Korea
[b] Department of Materials Science and Engineering, Korea University, Seoul, 02841, Republic of Korea
[c] Department of Energy Environment Policy and Technology, Green School, Graduate School of Korea Energy and Environment, Korea University, Seoul, 02841, Republic of Korea
[d] LG Electronics, Cheongju, 28431, Republic of Korea

A B S T R A C T

For screen-printed silicon solar cells, optimization of the contact characteristics between the front metal electrode and silicon is very significant for realizing high efficiency. As technology advances, the solar cell efficiency has been steadily increased. Especially, as surface recombination becomes more important in high efficiency solar cells, understanding and controlling recombination in the metal contact area are necessary. Recombination at the metal-silicon interface is a major cause of the drop in the open-circuit voltage (V_{oc}) of a solar cell. Thus far, the study of electrodes in silicon solar cells has been largely aimed at reducing the series resistance, and few studies on recombination due to electrodes have been performed. Quantitatively evaluating the recombination in electrodes to assess the effect on the efficiency is expected to become more important in the near future. In this paper, the contact characteristics of a screen-printed silver electrode and silicon interface were analyzed using saturation current density (J_o) measurements according to the surface doping concentration and firing temperature. The effects of the contact characteristics on V_{oc} and recombination were also investigated. Experimental results showed that $J_{o.pass}$ decreased with decreasing surface doping concentration and $J_{o.metal}$ increased with increasing surface doping concentration and firing temperature. For quantitative analysis of $J_{o.metal}$, the size and distribution of Ag crystallites were observed using SEM and TEM, and the Ag concentration was analyzed by ICP-OES measurements. The larger $J_{o.metal}$ was, the higher the Ag crystallite concentration, indicating that the Ag crystallites under the electrode increased $J_{o.metal}$. The effect of $J_{o.metal}$ on the electrical characteristics of the solar cell was analyzed by calculating the change in the surface recombination velocity and the decreased width of V_{oc}. Through this study, the recombination in the metallized area, which is expected to become increasingly important, and particularly the effects of the doping profile of the emitter region and silver crystallites on the surface recombination were quantitatively assessed. The amount of silver crystallites on the silicon wafer was quantitatively analyzed.

1. Introduction

In crystalline silicon solar cells, the front metal electrode seriously affects the series resistance, shadowing loss, fill factor and short-circuit current. The metal-silicon interface contributes to the surface recombination velocity (S_{eff}) of minority carriers, which limits the open-circuit voltage (V_{oc}) and achievable efficiency [1–5]. To minimize S_{eff} in metallized areas, controlling not only the doping concentration but also the contact characteristics between the metal and the diffused silicon is important [6–8]. A heavily doped silicon emitter has a low contact resistance with an electrode, but its use can diminish the electrical characteristics of a solar cell due to the increased Auger recombination, the low blue response, and recombination via crystal defects on the dead layer [9–13]. Decreasing the surface doping concentration is important for reducing surface recombination, but a reduction in the surface doping concentration may increase the contact resistance at the metal-silicon interface; therefore, optimization is necessary. Recently, many studies have been carried out to improve the contact characteristics in the low doping regime [14–19]. The carrier recombination for various doping concentrations in the emitter layer is characterized by the emitter saturation current density ($J_{o.emtter}$). $J_{o.emitter}$ consists of the saturation current densities in the passivation area ($J_{o.pass}$) and in the metallized area ($J_{o.metal}$) [5]. $J_{o.pass}$ depends on the doping concentration and can be obtained from quasi-steady-state photoconductance

* Corresponding author.
** Corresponding author.
*** Corresponding author.
E-mail addresses: lhseok@korea.ac.kr (H.-S. Lee), hsong@kier.re.kr (H.-e. Song), separk@kier.re.kr (S. Park).

https://doi.org/10.1016/j.solmat.2020.110519
Received 15 July 2019; Received in revised form 12 March 2020; Accepted 16 March 2020
Available online 21 March 2020

(QSSPC) measurements with both-side-doped and passivated silicon wafers. However, $J_{o.metal}$ cannot be measured directly, unlike $J_{o.pass}$, and should be evaluated considering the loss mechanism of the metal electrode based on the saturation current density measured in solar cells with various metal contact areas [20–22]. The metal contact area can be changed by altering the finger width or finger spacing, and recombination due to other factors should be controlled. In this paper, $J_{o.metal}$ was extracted and analyzed to identify the cause of carrier recombination at metal and silicon interfaces.

$J_{o.metal}$ has generally been extracted using the one-diode model. This method extracts $J_{o.metal}$ by using the slope of the saturation current density versus metal contact area plot and the J_{o1} obtained from Suns-Voc measurements [20–22]. This method has the limitation that m should be close enough to 1 to ignore the effect of J_{o2} and to extract $J_{o.metal}$ based only on the effect of J_{o1}. In addition, the drawback of separately preparing samples for obtaining the $J_{o.bulk}$ and $J_{o.BSF}$ required for the formula arises. Using the method of extracting $J_{o.metal}$ from QSSPC measurements proposed in this study, the above mentioned problem was solved. Samples for QSSPC measurements were fabricated with a symmetric structure, and samples with different doping profiles were produced by varying the $POCl_3$ deposition time and temperature. Each sample was classified into Group A, Group B or Group C, and the relationship between the surface doping concentration and $J_{o.metal}$ was investigated. After the doping process, passivation layers were deposited on both sides of the samples, and metal electrodes were formed in a pattern for measuring $J_{o.metal}$ using a screen printing method, followed by a firing process.

The surface doping concentration and the electrode formation temperature were varied to study the contact characteristics between the metal electrode and silicon, and the crystallite shape of the metal electrode was observed by scanning electron microscopy (SEM) and transmission electron microscopy-energy dispersive spectroscopy (TEM-EDS). Quantitative analysis of Ag crystallites in the metallized areas was also performed. Based on the shape of the crystallites and the extracted $J_{o.metal}$, the changes in the V_{oc} and S_{eff} of solar cells were analyzed and compared.

2. Experimental

The silicon substrate was a 6″ p-type Cz wafer from Longi with a resistivity of 1 ~ 3 Ω cm and a thickness of ~180 μm. The silicon wafers were textured using an alkaline solution and then doped in a tube furnace using a $POCl_3$ source. Doping led to the formation of emitter layers with sheet resistances of 60, 85 and 120 Ω/sq. Samples with n^+pn^+ structures doped with phosphorous on both sides were fabricated on p-type wafers. After the formation of the n^+pn^+ structure, the phosphorus silicate glass (PSG) formed in the diffusion process was removed by immersion in a 10 % HF solution for 30 s. Samples of three different structures were prepared to measure bulk lifetime, $J_{o.pass}$ and $J_{o.metal}$. To measure the bulk lifetime, the doping layer was removed by immersing the sample without PSG in 10 % KOH solution at 80 °C for 800 s and a high quality passivation layer was formed as Al_2O_3/SiN_x layer on the both side. The passivation layer with a thickness of ~ 10 nm Al_2O_3 and ~80 nm SiN_x was deposited on both sides using atomic layer deposition (ALD) and plasma enhanced chemical vapor deposition (PECVD), respectively. The sample for $J_{o.pass}$ measurement were deposited with ~80 nm SiN_x on both sides of the PSG-removed Si wafers using PECVD. The samples for $J_{o.metal}$ measurements were prepared with an electrode pattern of 5–25 % metal contact on the SiN_x deposited Si wafers using a screen printing method with Ag paste. All of the samples were fired at high temperature using a belt furnace. The peak temperatures were set to 875, 925 and 975 °C. The samples to measure bulk lifetime and $J_{o.pass}$ were 6″ wafer size. The electrode pattern for $J_{o.metal}$ samples was 4 × 4 cm^2, and nine electrode patterns were printed on one side of a 6″ wafer. After firing, $J_{o.metal}$ samples were cut along the electrode pattern using a laser. After laser cutting, the samples were immersed in 67 % nitric acid solution for 15 min to remove the bulk region of the electrode. J_o values were obtained in this study from quasi-steady-state photoconductance (QSSPC) measurements because the J_o of a SiN_x passivated sample can be easily and accurately obtained [23,24].

The dopant concentration of the doped emitter layer was measured by secondary ion mass spectrometry (SIMS). The distribution and size of the Ag crystallites formed on the surface were observed by SEM and quantitatively analyzed by inductively coupled plasma optical emission spectrometry (ICP-OES). The contact resistance between the silicon and metal was measured using the transfer length method (TLM), and the surface of the metal and silicon interface was observed using TEM. In addition, QSSPC data were utilized to calculate changes in V_{oc} and recombination velocities.

3. Results and discussion

3.1. Saturation current density and contact resistance

Surface recombination in crystalline silicon solar cells is considerably affected by the emitter doping profile [21,25–28]. For an electrode formed with a metal paste, contact is created between the metal and silicon under a high-temperature firing process. In this process, the recombination of carriers at the metal-silicon interface increases, resulting in a drop in V_{oc}. In this paper, the distribution and size of Ag crystallites in metal electrodes formed by varying the doping profile and the firing temperature were observed, and the surface recombination velocities at the metal-emitter interface were calculated. The $J_{o.metal}$ of the front electrode was obtained by fitting the saturation current density (J_o) as a function of the metal fraction with equations (1) and (2) [20,29]. Fig. 1 shows this plot for the Group A, B and C samples fired at 925 °C.

$$J_o = J_{o.bulk} + J_{or.pass} + J_{of.metal}(f) + J_{of.pass}(1-f) \quad (1)$$

$$\text{Slope} = J_{of.metal} - J_{of.pass} \quad (2)$$

$J_{o.pass}$ represents the saturation current density of the emitter when no metal electrode is present, and $J_{o.metal}$ is the sum of the slope of the plot and $J_{o.pass}$. The doping profiles of the fabricated samples were measured using SIMS, and the surface doping concentrations were 8.82 × 10^{20} cm^{-3} for Group A, 6.24 × 10^{20} cm^{-3} for Group B and 2.11 × 10^{20} cm^{-3} for Group C (Fig. 2). The sheet resistances were 60 Ω/sq. for Group A, 120 Ω/sq. for Group B, and 85 Ω/sq. for Group C. The $J_{o.pass}$ values were obtained from QSSPC measurements of samples deposited with ~80 nm SiN_x on both sides of the 6″ doped silicon wafers, and the results

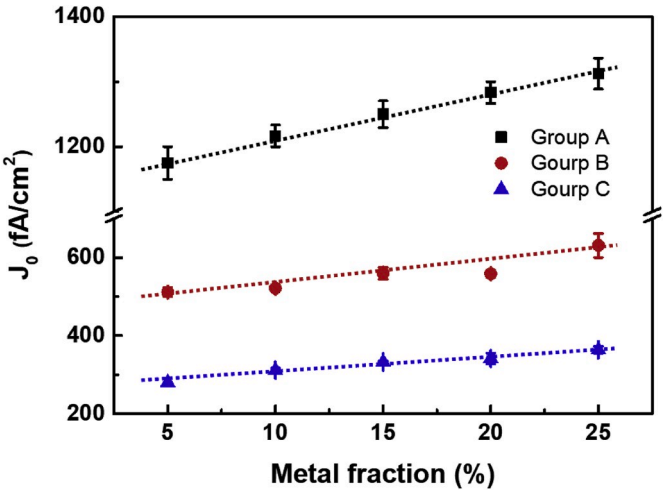

Fig. 1. Plot of J_o versus metal fraction used to determine $J_{o.metal}$ using QSSPC measurements for Group A,B and C samples at 925 °C firing temperature.

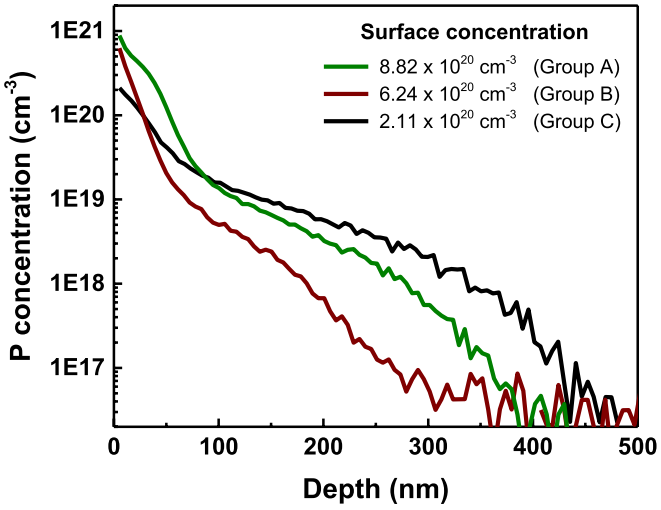

Fig. 2. SIMS profiles for various surface phosphorous concentrations on the silicon wafers.

are shown in Fig. 3. $J_{o.pass}$ was 250 fA/cm^2 for Group A, 93 fA/cm^2 for Group B and 48 fA/cm^2 for Group C. As the surface doping concentration on the sample surface decreased, $J_{o.pass}$ remarkably decreased. $J_{o.pass}$ was more dependent on the surface doping concentration than on the junction depth.

The firing temperatures were set to 875, 925 and 975 °C to examine not only the effect of the surface doping concentration but also the effect of the Ag crystallites formed during the firing process on the recombination property. Fig. 4 shows the $J_{o.metal}$ values for samples fired at the three different temperatures, and the results for samples fired at the same temperature are shown with the same pattern in the figure. In the case of p-type silicon solar cells, the J_o fitting at a low injection level is not good due to the LID of the wafer and the bulk degradation phenomenon caused by impurities. In this paper, $J_{o.metal}$ was extracted by fitting J_o at a high injection level. $J_{o.metal}$ decreased as the surface doping concentration of the emitter decreased, and $J_{o.metal}$ tended to increase with increasing firing temperature. $J_{o.metal}$ depended on the surface doping concentration, which indicated that the J_o of the front side of a solar cell was influenced more by the surface doping concentration than the junction depth.

To investigate the cause of the $J_{o.metal}$ change, the surface of the

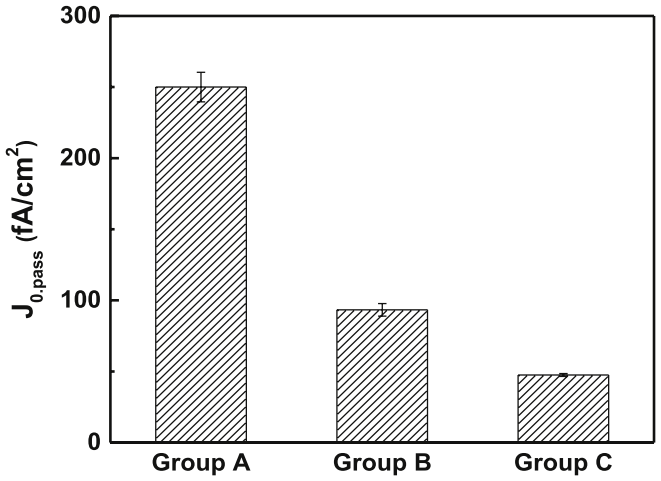

Fig. 3. Emitter saturation current density ($J_{o.pass}$) of symmetrically doped and SiN_x passivated Si wafers from QSSPC measurements as a function of the emitter surface concentration.

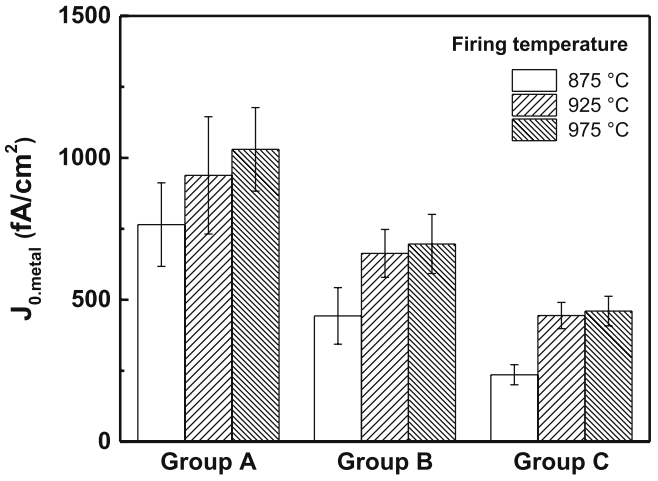

Fig. 4. Saturation current density of the metallized area ($J_{o.metal}$) for various surface doping concentrations and firing temperatures.

silicon was observed by SEM after removing the Ag bulk and glass frit from the sample after the firing process. The Ag concentration was quantitatively analyzed using ICP-OES after the samples were immersed in a 9.3 % nitric acid solution for 1 h to allow the sample's Ag crystallites to sufficiently dissolve in the solution. The SEM and ICP-OES measurement results are shown in Figs. 5 and 6. The size and distribution of Ag crystallites on the surface of samples with various firing temperatures were confirmed using SEM. The amount of Ag crystallites was quantitatively analyzed by ICP-OES, and the Ag concentration decreased as the surface doping concentration and firing temperature decreased. Fig. 6 shows that the Ag crystallite concentration tended to decrease as the silicon surface doping concentration became lower at all firing temperatures. This means that surface doping concentration and firing temperature influenced the formation of Ag crystallite. Previous studies have shown only qualitative relationship between Ag crystallite and surface doping concentration [6,16]. However, in this paper, the relationship between Ag crystallite and surface doping concentration was quantitatively confirmed by ICP-OES measurement. Based on these results, not only the surface doping concentration of the solar cell but also the size and distribution of the Ag crystallites formed during the firing process affect the carrier recombination.

To more precisely understand the formation of Ag crystallites according to the firing temperature, the interface between the Ag crystallites and silicon was observed by TEM and analyzed by EDS mapping. The Group C samples fired at 875 °C had a small amount of Ag crystallites of small size, as shown in Fig. 7. The Ag crystallite size increased with increasing firing temperature. The glass frit fluidity increased with the firing temperature, and the glass frit with fluidity flowed from the metal paste to the passivation layer. At this time, the PbO dissolved in the fluidized glass frit etched the passivation layer, exposing the emitter layer of the silicon surface [30,31]. Then, the etching reaction with the passivation layer proceeded, and the silicon was etched according to equations (3) and (4) [32].

$$2PbO_{(in\ glass)} + SiN_{x(s)} \rightarrow 2Pb_{(l)} + SiO_{2(in\ glass)} + x/2N_{2(g)} \quad (3)$$

$$2PbO_{(in\ glass)} + Si_{(s)} \rightarrow 2Pb_{(l)} + SiO_{2(in\ glass)} \quad (4)$$

The silicon at the exposed emitter surface and the Ag^+ ions in the glass frit formed Ag crystallites, as shown in equation (5), and the Ag crystallites formed an electrical contact with the emitter layer of the solar cell [32,33].

$$2Ag_2O_{(in\ glass)} + Si_{(s)} \rightarrow 4Ag_{(s)} + SiO_{2(in\ glass)} \quad (5)$$

A higher firing temperature resulted in faster etching of silicon and a

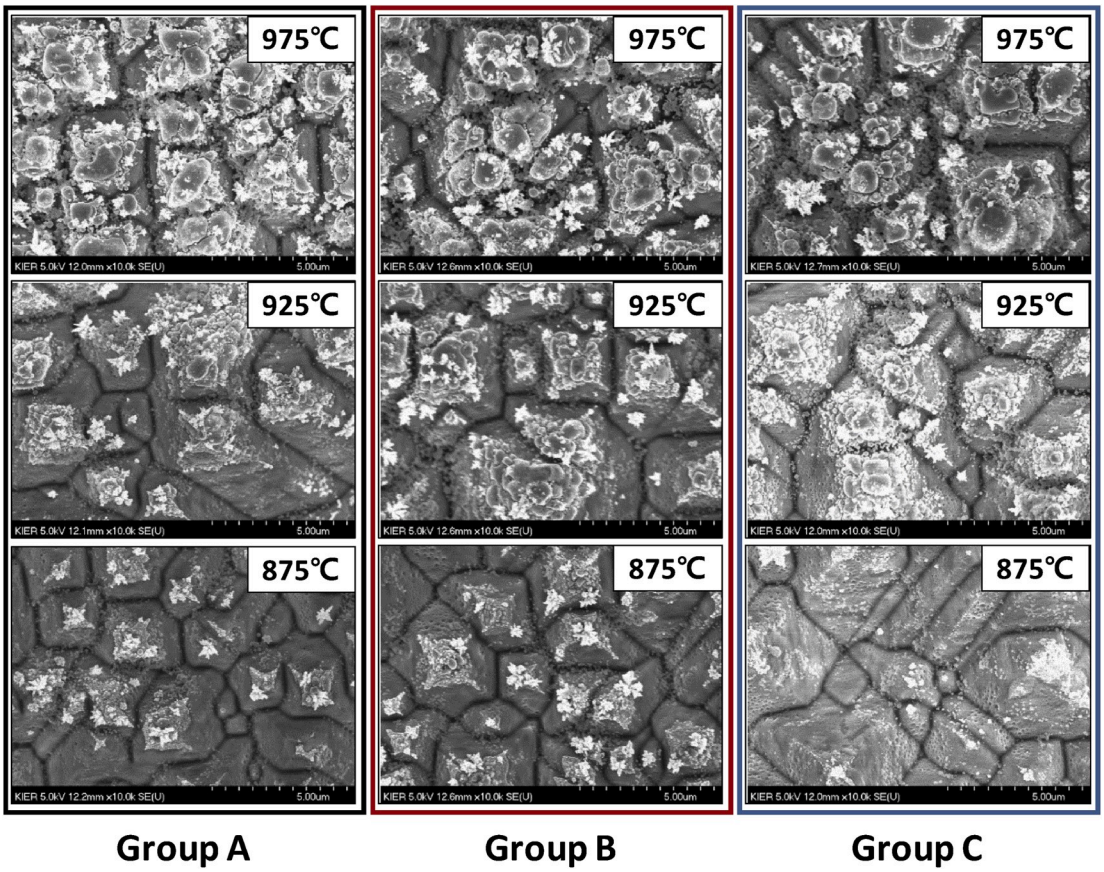

Fig. 5. SEM images of silicon surfaces after removal of the Ag metal bulk and glass frits from fired electrode silicon substrates with various surface doping concentrations and firing temperatures.

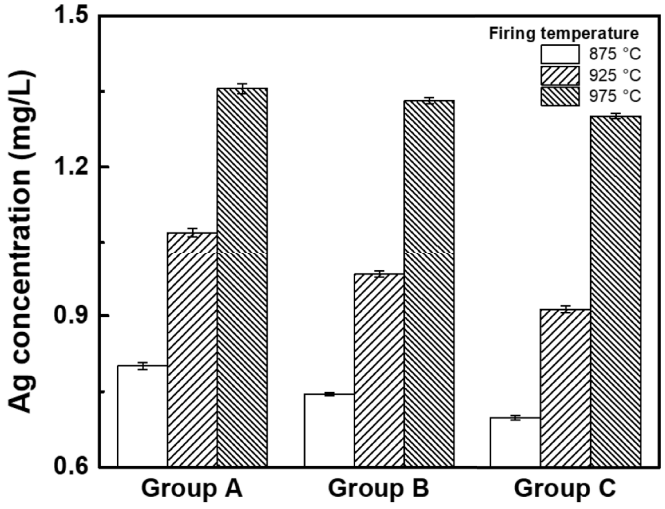

Fig. 6. ICP-OES measurements of Ag crystallites on silicon surfaces after removal of the Ag metal bulk and glass frits from fired electrode silicon substrates with various surface doping concentrations and firing temperatures.

larger size of the etch pits, and crystallization of the Ag precipitates in the etch pits occurred during cooling [33]. However, if the temperature was too low, then most Ag ions did not react with silicon and crystallized inside the glass layer. As shown in the TEM-EDS results in Fig. 7, at 875 °C, the Ag ions did not react with silicon and crystallized inside the glass due to the insufficient firing temperature. However, at 975 °C, the Ag crystallite size and the contact area with Si were large. These factors might cause carrier recombination at the crystalline silicon surface and increase $J_{o.metal}$ and the series resistance. The contact resistance was measured using the TLM method to determine the effect of the formation of Ag crystallites on the electrical contact at the metal-silicon interfaces. As shown in Fig. 8, the contact resistance increased with decreasing surface doping concentration and was highest at the highest firing temperature. An increase in the etching rate caused the formation of Ag crystallites that penetrated through the Si emitter layer to a bulk depth, thereby increasing the contact resistance. The depth direction of the formed Ag crystallites can be observed in the TEM image in Fig. 7, and the image confirmed that the Ag crystallites formed at 975 °C were deeper.

Referring to the TEM images in Fig. 7, the depth of the Ag crystallites was roughly estimated and correlated with the TLM results. By comparing the Ag crystallite depth and SIMS profiles, the correlation between the surface doping concentration and contact resistance could be analyzed. When the contact depth of the formed Ag crystallites was matched to the doping profile obtained by SIMS measurements, Ag crystallites were observed at contact depths of 24 nm and 44 nm, respectively, at 925 °C and 975 °C. Ag crystallite was not sufficiently formed at 875 °C firing temperature, so the contact depth could not be measured. The Ag crystallites were in contact with approximate concentrations of 1.23×10^{20} cm^{-3} at 925 °C and 4.75×10^{19} cm^{-3} at 975 °C. This result showed that when the electrode was formed at a high temperature, the Ag crystallite contact had a higher contact resistance due to the lower doping concentration.

3.2. V_{oc} calculation according to $J_{o.metal}$

The effect of increasing the contact area at the metal-silicon interfaces on the saturation current density and the drop in V_{oc} was

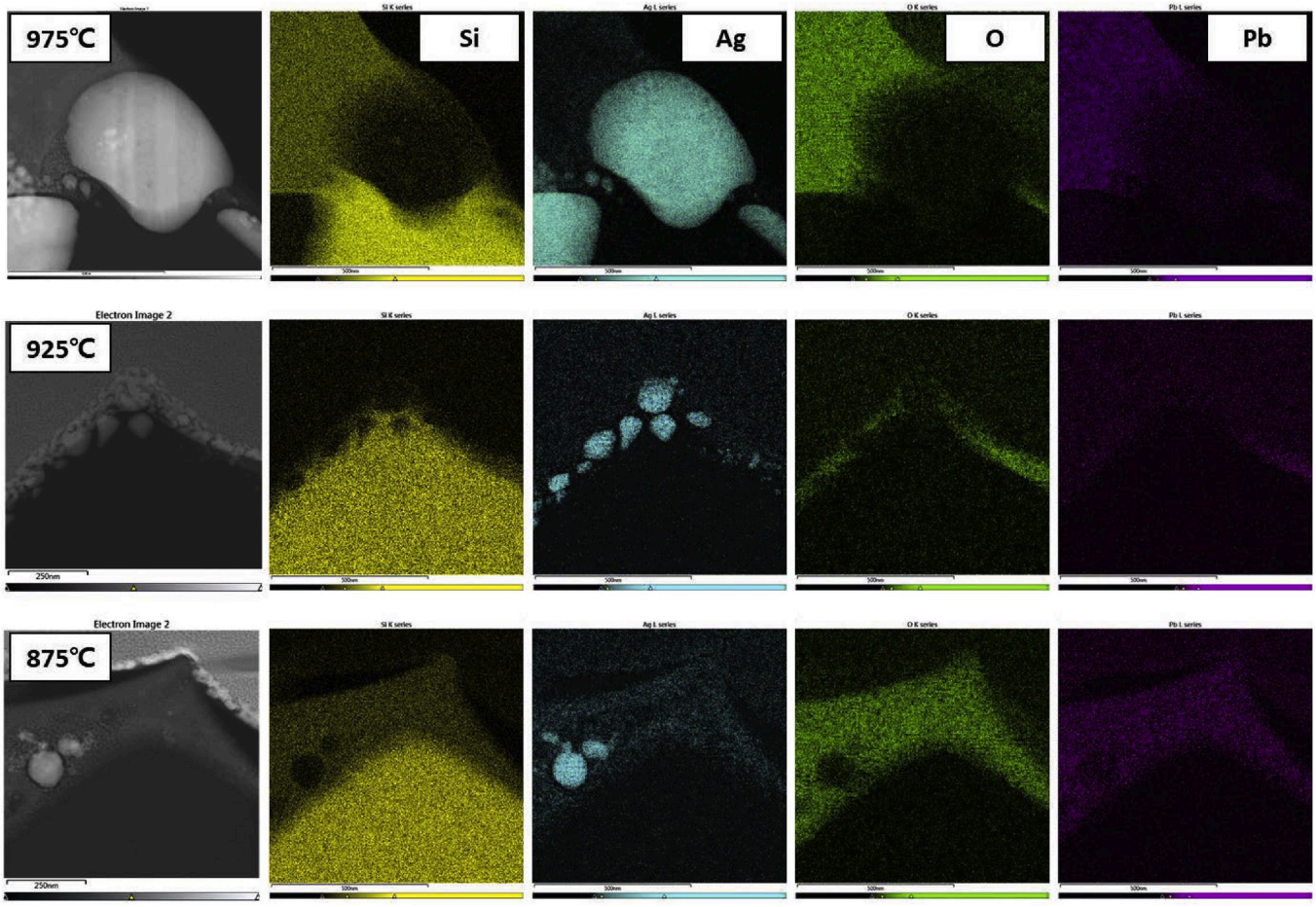

Fig. 7. TEM-EDS mapping images at the interface of the silicon and metal contact for Group C samples.

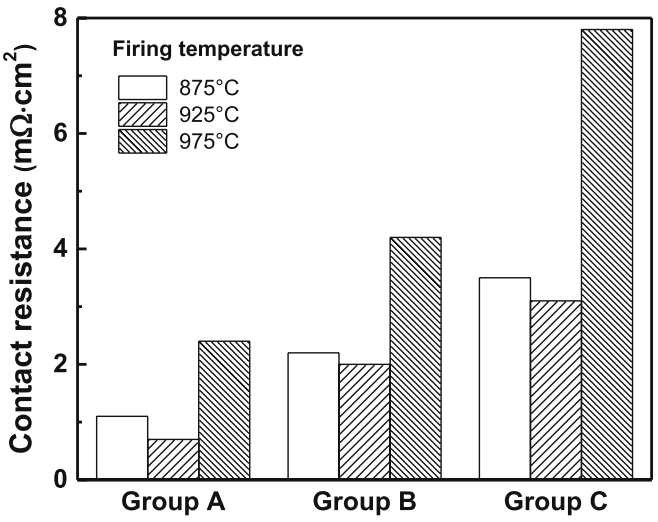

Fig. 8. Contact resistances from TLM measurements of the metal electrodes for various surface doping concentrations and firing temperatures.

investigated using the following calculations. The V_{oc} of a solar cell is expressed by equation (6), and V_{oc} is affected by J_o [34,35].

$$V_{oc} = \frac{kT}{q} \ln\left(\frac{J_{sc}}{J_0}\right) \tag{6}$$

where J_o is the sum of $J_{o.emitter}$ and the bulk saturation current density, $J_{o.b}$, as shown in equation (7) [34,35].

$$J_o = J_{o.emitter} + J_{o.b} \tag{7}$$

$$J_{o.emitter} = (1-f) \times J_{o.pass} + f \times J_{o.metal} \tag{8}$$

$$J_{o.b} = J_{o.bL} \left[\frac{J_{0.r} + J_{o.bL} \tanh\left(\frac{W_B}{L_B}\right)}{J_{0.bL} + J_{o.r} \tanh\left(\frac{W_B}{L_B}\right)}\right] \tag{9}$$

$$J_{o.bL} = \frac{qDn_i^2}{N_A L_B} \tag{10}$$

where $J_{o.b}$ is the base saturation current, $J_{o.bL}$ is the bulk-lifetime-dependent saturation current, $J_{o.r}$ is the rear side saturation current, W_B is the wafer thickness, L_B is the diffusion length, q is the electronic charge, D is the diffusion coefficient, n_i is the intrinsic carrier concentration and N_A is the doping concentration. $J_{o.bL}$ was calculated using equation (10), and the diffusion length was calculated after obtaining the bulk lifetime of the sample through experiments. To measure the bulk lifetime of the wafers, the doped layer was removed in doped wafers and the effective lifetime was measured using QSSPC after depositing a high quality passivation layer of Al_2O_3/SiN_x layer on both sides of wafers. The bulk lifetime was calculated using equations (11) and (12) [36,37].

$$J_{o.emitter} = \frac{S_{eff}}{qn_i^2} \times (N_A + \Delta n) \tag{11}$$

$$\frac{1}{\tau_{bulk}} = \frac{1}{\tau_{eff}} - \frac{2S_{eff}}{W} \quad (12)$$

where W is the sample thickness, S_{eff} is the effective surface recombination velocity and Δn is the excess carrier concentration. The S_{eff} values of Group A and Group B were calculated as 9.8 cm/s and Group C as 10.1 cm/s at the commonly used 10^{15} cm^{-3} injection level [36]. As a result, the bulk lifetime were ~343 μs for Group A, B and ~241 μs for Group C. Subsequently, $J_{o.b}$ was calculated using equation (9), and $J_{o.r}$ was 74 fA/cm^2, based on QSSPC measurements. J_o was obtained using the $J_{o.pass}$ and $J_{o.metal}$ values mentioned previously, and V_{oc} according to the metal fraction was calculated by substituting this value into equation (6). J_{sc} was 39 mA/cm^2. As shown in Fig. 9, V_{oc} decreased as the metal fraction increased. $J_{o.metal}$ increased as the contact area between the Ag crystallites and the silicon surface increased, resulting in a decrease in V_{oc}. Additionally, as the surface doping concentration decreased, V_{oc} increased from ~656 mV to ~673 mV for 0% metal fraction at 925 °C firing temperature. Thus, a decrease in $J_{o.emitter}$ resulted in an increase in V_{oc} by decreasing the total J_o in equation (6).

In all the surface doping concentration conditions, V_{oc} decreased as the firing temperature increased, and the decrease in V_{oc} was greater as the metal fraction increased. V_{oc} decreased by 1.3 ~ 2.1 mV as the metal fraction increased by 5% at 875 °C but decreased by 2.2 ~ 3.2 mV at 925 °C and 975 °C. As mentioned in the previous section, the amount of formed Ag crystallites was small at 875 °C, and thus, the decrease in V_{oc} was considered to be small even if the metal fraction increased. In contrast, at 925 °C and 975 °C, the Ag crystallite size and the contact area with Si were large, and the effect of $J_{o.metal}$ was greater than that at 875 °C, where fewer Ag crystallites formed. This result was mainly due to the size and distribution of Ag crystallites.

4. Conclusion

In this paper, the relationship between the recombination loss and V_{oc} was investigated according to the conditions of contact formation between a metal electrode and a silicon substrate. $J_{o.metal}$ was extracted, and the surface doping concentration and firing temperature were found to have a great influence. $J_{o.metal}$ showed a tendency to increase as the surface doping concentration of the solar cell and the firing temperature increased. Based on SEM images of the solar cell surfaces, increasing the firing temperature affected the size and distribution of Ag crystallites. For quantitative measurement, the concentration of Ag crystallites was measured using ICP-OES, and the Ag concentration increased with increasing firing temperature and surface doping concentration. The increase in the amount of Ag crystallites lowered the contact resistance. However, the contact resistance increased at 975 °C because excessive silicon etching by the Ag ions contained in the fluidized glass frit caused damage to the emitter layer and increased the contact area at the metal-silicon interface. V_{oc} was significantly influenced by the surface doping concentration of the solar cell and the amount of Ag crystallites at the metal-silicon interface. V_{oc} decreased with increasing surface doping concentration and metal electrode fraction. In this paper, QSSPC measurements were used to extract $J_{o.metal}$ based on an accurate $J_{o.pass}$. However, the extraction of $J_{o.metal}$ using QSSPC measurements was less accurate in the low injection region due to the effect of surface recombination. This behavior became worse at higher firing temperatures. In this work, we extracted $J_{o.metal}$ in the high injection region. Therefore, to extract $J_{o.metal}$ more precisely, J_{o1} and J_{o2} should be analyzed together to improve the accuracy. This analysis will be performed in future investigations.

Declaration of competing interest

The authors declare that they have no known competing financial interests or personal relationships that could have appeared to influence the work reported in this paper.

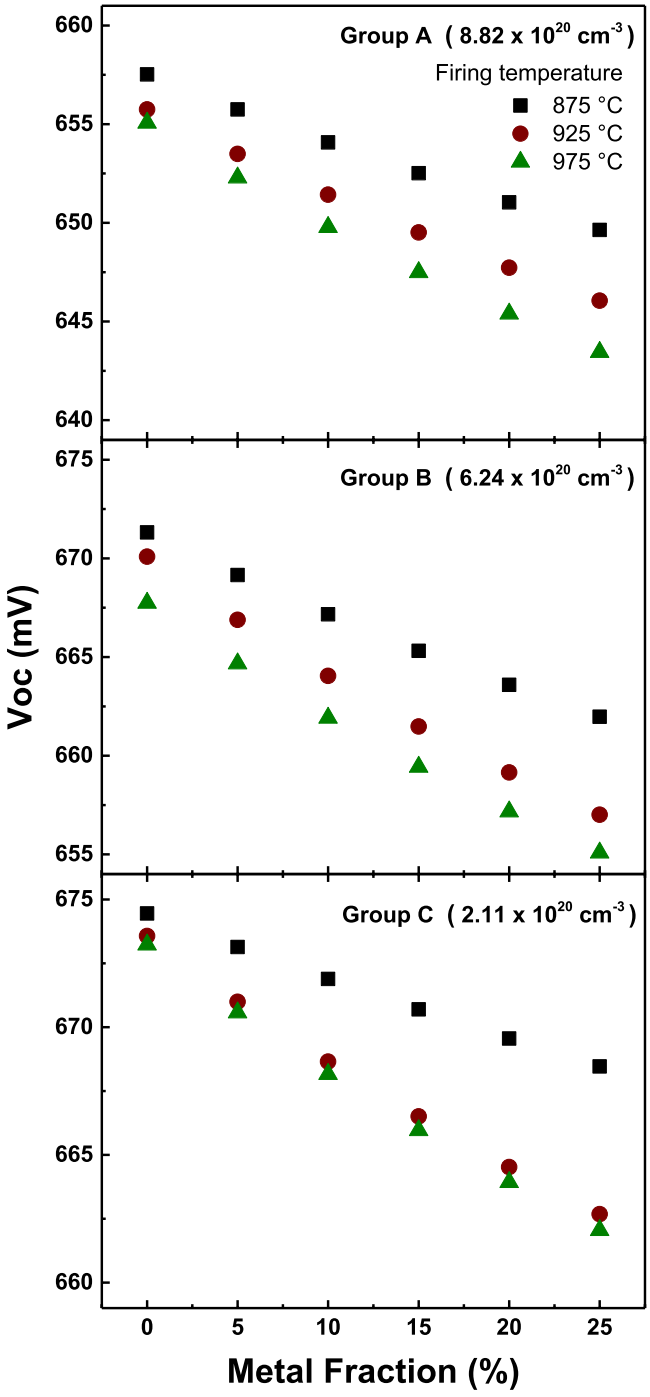

Fig. 9. Calculated open-circuit voltages as a function of the metal fraction for various surface doping concentrations and firing temperatures.

CRediT authorship contribution statement

Myeong Sang Jeong: Conceptualization, Methodology, Investigation, Writing - original draft. **Kwan Hong Min:** Data curation, Investigation. **Sungjin Choi:** Investigation. **Min Gu Kang:** Formal analysis. **Kyung Taek Jeong:** Resources. **Eun Tae Lee:** Resources. **Yoonmook Kang:** Data curation. **Donghwan Kim:** Supervision. **Hae-Seok Lee:** Writing - review & editing, Supervision. **Hee-eun Song:** Writing - review & editing, Supervision. **Sungeun Park:** Conceptualization, Writing - review & editing, Supervision.

Acknowledgements

This work was conducted under the framework of the Research and Development of the Korea Institute of Energy Research (C0-2402); the New and Renewable Energy Technology Development Program of the Korea Institute of Energy Technology Evaluation and Planning (KETEP) through a grant funded by the Ministry of Knowledge Economy, Korea (Project No. 20193010014530); and the Technology Development Program to Solve Climate Changes of the National Research Foundation (NRF) funded by the Ministry of Science, ICT & Future Planning (2017M1A2A2086911).

Appendix A. Supplementary data

Supplementary data to this article can be found online at https://doi.org/10.1016/j.solmat.2020.110519.

References

[1] S.E.E. Profile, Analysis of the Emitter Saturation Current Density of Industrial Type Silver Screen-Printed Front Contacts Analysis of the Emitter Saturation Current Density of Industrial, 2015, pp. 2–6, https://doi.org/10.4229/27thEUPVSEC2012-2BV.5.10.

[2] B. Min, A. Dastgheib-Shirazi, P.P. Altermatt, H. Kurz, Accurate determination of the emitter saturation current density for industrial P-diffused emitters, in: Proc. 29th Eur. Photovolt. Sol. Energy Conf. Exhib. Amsterdam, Netherlands, 2014, pp. 463–466, https://doi.org/10.4229/EUPVSEC20142014-2BO.3.6.

[3] R. Hoenig, M. Glatthaar, F. Clement, J. Greulich, J. Wilde, D. Biro, New measurement method for the investigation of space charge region recombination losses induced by the metallization of silicon solar cells, Energy Procedia 8 (2011) 694–699, https://doi.org/10.1016/j.egypro.2011.06.203.

[4] J. Müller, K. Bothe, S. Gatz, F. Haase, C. Mader, R. Brendel, Recombination at laser-processed local base contacts by dynamic infrared lifetime mapping, J. Appl. Phys. 108 (2010), https://doi.org/10.1063/1.3517109.

[5] C. Reichel, F. Granek, J. Benick, O. Schultz-Wittmann, S.W. Glunz, Comparison of emitter saturation current densities determined by injection-dependent lifetime spectroscopy in high and low injection regimes, Prog. Photovoltaics Res. Appl. (2012), https://doi.org/10.1002/pip.942.

[6] M.M. Hilali, S. Sridharan, C. Khadilkar, A. Shaikh, A. Rohatgi, K.I.M. Steve, Effect of glass frit chemistry on the physical and electrical properties of thick-film Ag contacts for silicon solar cells, J. Electron. Mater. 35 (2006) 2041–2047, https://doi.org/10.1007/s11664-006-0311-x.

[7] P.N. Vinod, Specific contact resistance and carrier tunneling properties of the silver metal/porous silicon/p-Si ohmic contact structure, J. Alloys Compd. 470 (2009) 393–396, https://doi.org/10.1016/j.jallcom.2008.02.110.

[8] M. Hörteis, T. Gutberlet, A. Reller, S.W. Glunz, High-Temperature contact formation on n-Type silicon: basic reactions and contact model for Seed-Layer contacts, Adv. Funct. Mater. 20 (2010) 476–484, https://doi.org/10.1002/adfm.200901305.

[9] V. Shanmugam, A. Khanna, P.K. Basu, A.G. Aberle, T. Mueller, J. Wong, Impact of the phosphorus emitter doping profile on metal contact recombination of silicon wafer solar cells, Sol. Energy Mater. Sol. Cells 147 (2016) 171–176, https://doi.org/10.1016/j.solmat.2015.12.006.

[10] A. Cuevas, D.A. Russell, Co-optimisation of the emitter region and the metal grid of silicon solar cells, Prog. Photovoltaics Res. Appl. 8 (2000) 603–616, https://doi.org/10.1002/1099-159X(200011/12)8:6<603::AID-PIP333>3.0.CO;2-M.

[11] B. Min, H. Wagner, A. Dastgheib-Shirazi, A. Kimmerle, H. Kurz, P.P. Altermatt, Heavily doped Si: P emitters of crystalline Si solar cells: recombination due to phosphorus precipitation, Phys. Status Solidi Rapid Res. Lett. 8 (2014) 680–684, https://doi.org/10.1002/pssr.201409138.

[12] H. Wagner, A. Dastgheib-Shirazi, B. Min, A.E. Morishige, M. Steyer, G. Hahn, C. Del Cañizo, T. Buonassisi, P.P. Altermatt, Optimizing phosphorus diffusion for photovoltaic applications: peak doping, inactive phosphorus, gettering, and contact formation, J. Appl. Phys. 119 (2016), https://doi.org/10.1063/1.4949326.

[13] A. Lanterne, S. Gall, S. Manuel, R. Monna, D. Ramappa, M. Yuan, P. Rivalin, A. Tauzin, Annealing, passivation and contacting of ion implanted phosphorus emitter solar cells, Energy Procedia 27 (2012) 580–585, https://doi.org/10.1016/j.egypro.2012.07.113.

[14] V. Shanmugam, J. Cunnusamy, A. Khanna, P.K. Basu, Y. Zhang, C. Chen, A. F. Stassen, M.B. Boreland, T. Mueller, B. Hoex, A.G. Aberle, Electrical and microstructural analysis of contact formation on lightly doped phosphorus emitters using thick-film ag screen printing pastes, IEEE J. Photovoltaics. 4 (2014) 168–174, https://doi.org/10.1109/JPHOTOV.2013.2291313.

[15] I.B. Cooper, K. Tate, J.S. Renshaw, A.F. Carroll, K.R. Mikeska, R.C. Reedy, A. Rohatgi, Investigation of the mechanism resulting in low resistance ag thick-film contact to si solar cells in the context of emitter doping density and contact firing for current-generation ag paste, IEEE J. Photovoltaics. 4 (2014) 134–141, https://doi.org/10.1109/JPHOTOV.2013.2285621.

[16] G. Schubert, J. Horzel, R. Kopecek, F. Huster, P. Fath, Silver thick film contact formation ON lowly doped phosphorous emitters, in: 20st Eur. Photovolt. Sol. Energy Conf. Exhib., 2005.

[17] S. Werner, E. Lohmüller, A. Wolf, F. Clement, Extending the limits of screen-printed metallization of phosphorus- and boron-doped surfaces, Sol. Energy Mater. Sol. Cells 158 (2016) 37–42, https://doi.org/10.1016/j.solmat.2016.05.064.

[18] S. Werner, E. Lohmüller, S. Maier, S. Mourad, A. Wolf, Challenges for lowly-doped phosphorus emitters in silicon solar cells with screen-printed silver contacts, Energy Procedia 124 (2017) 936–946, https://doi.org/10.1016/j.egypro.2017.09.274.

[19] M.Z. Burrows, A. Meisel, D. Balakrishnan, A. Tran, D. Inns, E. Kim, A.F. Carroll, K. R. Mikeska, Front-side Ag contacts enabling superior recombination and fine-line performance, in: Conf. Rec. IEEE Photovolt. Spec. Conf., 2013, https://doi.org/10.1109/PVSC.2013.6744905.

[20] D. Inns, D. Poplavskyy, Measurement of metal induced recombination in solar cells, in: 2015 IEEE 42nd Photovolt. Spec. Conf. PVSC 2015, 2015, pp. 1–4, https://doi.org/10.1109/PVSC.2015.7356056.

[21] T. Fellmeth, A. Born, A. Kimmerle, F. Clement, D. Biro, R. Preu, Recombination at metal-emitter interfaces of front contact technologies for highly efficient silicon solar cells, Energy Procedia 8 (2011) 115–121, https://doi.org/10.1016/j.egypro.2011.06.111.

[22] A. Edler, V.D. Mihailetchi, L.J. Koduvelikulathu, C. Comparotto, R. Kopecek, R. Harney, Metallization-induced recombination losses of bifacial silicon solar cells, Prog. Photovoltaics Res. Appl. (2015), https://doi.org/10.1002/pip.2479.

[23] R.A. Sinton, A. Cuevas, M. Stuckings, Quasi-steady-state Photoconductance, a New Method for Solar Cell Material and Device Characterization, 2002, https://doi.org/10.1109/pvsc.1996.564042.

[24] A. Cuevas, The effect of emitter recombination on the effective lifetime of silicon wafers, Sol. Energy Mater. Sol. Cells 57 (1999) 277–290, https://doi.org/10.1016/S0927-0248(98)00179-2.

[25] R.R. King, Studies of Diffused Phosphorus Emitters : Saturation Current, Surface Recombination Velocity, Quantum Efficiency, 1990, p. 37.

[26] A. Cuevas, P.A. Basore, G. Giroult-Matlakowski, C. Dubois, Surface recombination velocity of highly doped n-type silicon, J. Appl. Phys. 80 (1996) 3370–3375, https://doi.org/10.1063/1.363250.

[27] A. Cuevas, G. Giroult-Matlakowski, P.A. Basore, C. DuBois, R.R. King, Extraction of the Surface Recombination Velocity of Passivated Phosphorus-Doped Silicon Emitters, 2002, https://doi.org/10.1109/wcpec.1994.520221.

[28] M.J. Kerr, J. Schmidt, A. Cuevas, J.H. Bultman, Surface recombination velocity of phosphorus-diffused silicon solar cell emitters passivated with plasma enhanced chemical vapor deposited silicon nitride and thermal silicon oxide, J. Appl. Phys. 89 (2001) 3821–3826, https://doi.org/10.1063/1.1350633.

[29] I. Gordon, J. Szlufcik, Decreasing Metallization Related Recombinations For Screen Printed n-pert Cells By Selective Laser Doping and Reduction In Contact Fraction, (n.d.).

[30] C. Ballif, D.M. Huljić, G. Willeke, A. Hessler-Wyser, Silver thick-film contacts on highly doped n -type silicon emitters: structural and electronic properties of the interface, Appl. Phys. Lett. 82 (2003) 1878–1880, https://doi.org/10.1063/1.1562338.

[31] G. Schubert, F. Huster, P. Fath, Physical understanding of printed thick-film front contacts of crystalline Si solar cells-Review of existing models and recent developments, Sol. Energy Mater. Sol. Cells 90 (2006) 3399–3406, https://doi.org/10.1016/j.solmat.2006.03.040.

[32] K.K. Hong, S. Bin Cho, J.S. You, J.W. Jeong, S.M. Bea, J.Y. Huh, Mechanism for the formation of Ag crystallites in the Ag thick-film contacts of crystalline Si solar cells, Sol. Energy Mater. Sol. Cells 93 (2009) 898–904, https://doi.org/10.1016/j.solmat.2008.10.021.

[33] J. Qin, W. Zhang, S. Bai, Z. Liu, Study on the sintering and contact formation process of silver front side metallization pastes for crystalline silicon solar cells, Appl. Surf. Sci. 376 (2016) 52–61, https://doi.org/10.1016/j.apsusc.2016.03.089.

[34] S. Park, H. Park, Y. Kang, H.S. Lee, D. Kim, Analysis of aluminum back surface field at different wafer specifications in crystalline silicon solar cells, Curr. Appl. Phys. 16 (2016) 1062–1068, https://doi.org/10.1016/j.cap.2016.05.016.

[35] S. Bowden, D.S. Kim, C. Honsberg, A. Rohatgi, Rapid thermal processing for front and rear contact passivation, Conf. Rec. IEEE Photovolt. Spec. Conf. (2002) 410–413, https://doi.org/10.1109/PVSC.2002.1190546.

[36] M. Al-amin, N.E. Grant, A.I. Pointon, J.D. Murphy, Iodine – Ethanol Surface Passivation for Measurement of Millisecond Carrier Lifetimes in Silicon Wafers with Different Crystallographic Orientations, 2019, pp. 1–7, https://doi.org/10.1002/pssa.201900257, 1900257.

[37] A.G. Aberle, Surface passivation of crystalline silicon solar cells: a review, Prog. Photovoltaics Res. Appl. (2000), https://doi.org/10.1002/1099-159X(200009/10)8:5<473::AID-PIP337>3.0.CO;2-D.